Heliyon 6 (2020) e03389

Contents lists available at ScienceDirect

Heliyon

journal homepage: www.cell.com/heliyon

Research article

# Ferroelectric behavior and spectroscopic properties of La-Modified lead titanate nanoparticles prepared by a sol-gel method

M. Mostafa [a,b,*], Z.A. Alrowaili [a], G.M. Rashwan [b,c], M.K. Gerges [c]

[a] Physics Department, College of Science, Jouf University, Sakaka, Saudi Arabia
[b] Laser Tech. & Environment Lab., Physics Department, Faculty of Science, South Valley University, Qena, 83523 Egypt
[c] Ferroelectric Lap, Physics Department, Faculty of Science, South Valley University, Qena 83523, Egypt

ARTICLE INFO

*Keywords:*
Materials science
Nanotechnology
Ceramics
Ferroelectrics
PLT
Sol-gel
Optical
Dielectric

ABSTRACT

The sol-gel method was used to prepare perovskite type ($Pb_{1-1.5x}$ $La_x\square_{0.5x}$)$TiO_3$ (PLT) ceramics with x = 0.21, 0.22, 0.23, 0.24, 0.25 in order to investigate their structural, optical, and dielectric properties. The crystallite compounds were obtained by calcinating the mixture of $PbCO_3$, $TiO_2$, and $La_2O_3$ at 1000 °C for different time periods. After 4 h annealing, PLT23 sample, approximately a very little secondary phases have been observed in the XRD spectrum of the PLT sample with 23% La content (PLT23). The presence of La dopants might have affected the tetragonality of the Lead titanate crystal structure. The PLT samples tolerance factor decreases from 0.991 as in x = 0.21 to 0.986 for x = 0.25. Hence, these structures tend, generally, to be in the perovskite phase as t ~ 1. In the doped ceramics, characteristic phase transitions were shifted to lower temperatures. The dielectric permittivity value showed the tendency of a slight increase with lanthanum addition and achieved its maximum $\varepsilon_m$ (3649) at x = 0.23, then it decreases for higher concentrations of La. The samples' estimated average crystallite size ranged from 40 nm to 50 nm, the maximum crystallite size about (49.6 nm) at x = 0.23 La. The calculated bandgaps were 3.1, 3.26, 3.28, 3.08, and 3.12 for the PLT with 0.21, 0.22, 0.23,0.24 and 0.25% La, respectively. The Curie constant C was obtained as the slope of the curve of the inverse values of $\varepsilon_r$ vs. temperature. The highest C value ($5.2 \times 10^5$ K) was measured for the 23% La sample. The sample with 23% La content appears to be notably distinguished in its structural, optical, and dielectric characteristics compared with other samples.

## 1. Introduction

Due to the importance of the ferroelectric ceramics as electronic materials, they are applied in many industries such as capacitors, transducers, sensors, and ultrasonic motors [1]. Perovskite systems ($ABO_3$), a potential applicant as the ferroelectric materials, have attracted great research interests. The common structure of the perovskite materials is labeled as $ABX_3$, where the positions A and B are considered as cations with dissimilar sizes and both are bonded by X is an anion. The B atoms are usually smaller than the B atoms [2]. In general, semimetal or metal founded in the periodic table may replace A and B positions. In general, the anion can be any other one at this location as oxygen [3]. Perfectly, the perovskite structure is a cubic in its form. The corners of the cubic cells are occupied by A atoms, where the center is placed by B atoms, but the atoms of oxygen can be found in the centers of the faces. Atom in position A represents a larger radii or alkali earth metals lanthanide in perovskite cubic unit cell [4]. Generally, oxygen anions coordinate A cations that are 12-fold which occupy the corners of the cube with a corner position of (0, 0, 0), the cubic lattice's face center is occupied by oxygen atoms at the position of (½,½, 0); however, the body center is occupied by the B cations which lie inside the center of oxygen octahedral at the position (½, ½, ½) [5]. Lead titanate ($PbTiO_3$ or PT) ceramics were studied extensively as one of the important perovskite ferroelectric materials. The improvement in the piezoelectric and pyroelectric properties is achieved by replacing Pb in the A site of the $ABO_3$ structure [6, 7, 8]. The prominent $PbTiO_3$ with the perovskite crystal structure possesses a relatively high Curie point of 490 °C. The high c/a ratio in $PbTiO_3$ at low temperature confers tetragonal phase. So, it disintegrates into powder when cooled to the Curie point [9]. Various methods of $PbTiO_3$ nanopowder preparation, such as the conventional mixed-oxide method, Pechini-type processes, mechanochemical synthesis, hydrothermal process, sputtering, spray drying, and sol-gel processing have already been reported by some authors [10, 11, 12, 13, 14, 15, 16]. Among these methods, the low-cost

* Corresponding author.
*E-mail address:* mmostafa@ju.edu.sa (M. Mostafa).

https://doi.org/10.1016/j.heliyon.2020.e03389
Received 7 September 2019; Received in revised form 17 December 2019; Accepted 5 February 2020

and simple sol-gel technique can precisely control the composition, making it more advantageous.

Lanthanum (La) – modified lead titanate or lead lanthanum titanate (PLT) is an important ferroelectric material that is characterized with its excellent dielectric, ferroelectric, pyroelectric, and electro-optic properties. The resulting PLT's permittivity increases with Tc when doping $PbTiO_3$ nanopowders with La, while its tetragonality decreases with increasing La content [17]. The coercive field, that is required to polarize the ceramic drops, and a pyroelectric coefficient larger than that of PT, was observed [18]. Relaxor ferroelectrics based on lead with complex perovskite structure are commonly used in piezoelectric actuators, ultrasonic transducers, and multilayer capacitors because of their exceptional piezoelectric and dielectric properties [19, 20, 21, 22]. In lanthanum that contains lead titanate [23], $La^{3+}$ ions occupy $Pb^{2+}$ sites and produce vacancies ( □ ) in the cation lattice of ($Pb_{1-1.5x}$ $La_x$ '□ $_{0.5x}$) $TiO_3$ ceramics. The transition temperature $T_c$ decreases linearly with an increasing $La^{3+}$ content. Some ferroelectric properties of ceramics with previous chemical formulas have been investigated previously and related experimental and theoretical studies [24] noted that the dielectric peak $\varepsilon_{max}$ behavior is alike to the single vacancies at the same La content. It has been found that the maximum value of $\varepsilon_{max}$ at $x = 0.2$ compatible with the maximum number of single vacancies signifying that both the dielectric peak $\varepsilon_{max}$ and the number of single vacancies is relative to La content till the value reaches 20 %. Wu et al. [25] studied the perovskite structure with the general formula $ABO_3$ and found that the A site of vacancies decreases the local stress in the domains undergoing domain switching and the domain width is proportional to the crystallite size [26]. Many studies [ e.g., [27, 28, 29, 30, 31, 32, 33]] found that the increase in crystallite size was associated with the increasing dielectric peak $\varepsilon_{max}$.

Recently, lead titanate (PT) based ceramics has increasingly become one of the most ferroelectric materials that have been investigated and used in the scientific and industrial communities for its high Curie temperature (Tc) and low dielectric constant, which made it a valuable research object [34]. This research aimed at studying the microstructural, optical, and dielectric properties of PbTiO3 with various La-doping concentrations (i.e., x = 0.21, 0.22, 0.23, 0.24, and, 0.25 mol La, denoted as PLT21, PLT22, PLT23, PLT24, and PLT25, respectively).

## 2. Materials and methods

The ($Pb_{1-1.5x}$ $La_x$□$_{0.5x}$)$TiO_3$, where (x = 0.21, 0.22, 0.23, 0.24, and 0.25 mole La) nanoparticles were prepared by the sol-gel method. The raw materials used were commercially available lead carbonate ($PbCO_3$), titanium dioxide ($TiO_2$), and lanthanum oxide ($La_2O_3$), which were purchased from Alfa Aesar, a Johnson Matthey Co. Potassium hydroxide (KOH, 0.2 moles) was dissolved in 100 ml distilled water and 0.1 moles of $PbCO_3$ were added to the prepared KOH solution. The mixture was magnetically stirred for 1 h and then filtered. The solids retained on the filter was added to $La_2O_3$ with distilled water under stirring the mixture for 2h, finally, 0.1 moles of $TiO_2$ were added to 100 ml distilled water. The resultant mixture was magnetically stirred for 2 h to obtain a homogeneous solution (colloidal solution). Then, the mixture powders were calcined at the calcination temperature-which are chosen as appropriate calcination from previous work [14]- of 1000 °C, for 2 and 4 h at a heating/cooling rate of 5 °C/min. X-ray diffraction (XRD) was employed to identify the phase formed. The particle morphology and size were directly imaged by transmission electron microscopy (TEM); Scherrer equation is used to determine the average crystallite size. A powder of PLT consisted of 7 mm diameter and 1 mm thickness is compressed in a pellet. were prepared in order to be used in the investigation on the electrical properties. electrodes made of silver thin film were printed onto the two ceramic disk opposite faces. In order to remove the organic contamination, the printed disks were kept on an alumina plate, and heated for 2 h at 500 °C first. For measuring the pellets' capacitance, the heated disk was placed between two probes of copper connected to a computerized capacitance meter (RLC meter -model SRS) [32] (see Figure 1).

## 3. Results and discussion

### 3.1. X-ray diffraction

The XRD patterns were obtained for the powders calcined at 1000 °C using XRD (EMMA) diffractometer in the range of Bragg's angle (2θ) from 20° to 80°. According to the results shown in Figures 2 and 3, it is clear that, in the case of the sample calcined at 1000 °C for 2 h, crystallization started to form perovskite PLT phase along with small impurities of PbO and $TiO_2$. However, the impurity phases gradually decreased when annealed at 1000 °C for a longer period of time. As a result, after 4 h of calcination, the $TiO_2$ impurities disappeared in all PLT samples with La concentrations ranging from 21% to 25%. The sample with 23% La sintered at 1000 °C for 4 h showed the highest purity. The sharp intensity peak at $2\theta = 31.85°$ shows the formation of perovskite PLT phase; while approximately no peaks for the unwanted $TiO_2$ or PbO phases were observed in the XRD patterns except some little peaks that have a low intensity, which indicated that the sol-gel process used in this study was an appropriate technique for the preparation of PLT nanoparticles. The broad XRD peaks suggest the presence of nanocrystalline particles. Based on these XRD patterns, the Scherrer's equation was used to calculate the crystallite sizes (1):

$$t = 0.9\lambda/\beta\cos\theta \quad (1)$$

where λ is the wavelength, β is the full width at half maximum (FWHM), and θ is the diffraction angle. The calculated crystallite size was 45.5 nm, 44.6 nm, 49.6 nm, 40.3 nm, and 40.6 nm for the PLT with 0.21, 0.22, 0.23,0.24 and 0.25% La, respectively.

### 3.2. SEM analysis

Figure 4 shows the morphology and size distribution PLT powders of 21, 22, 23,24 and 25 % La, respectively. In general, the particles are spherical in their morphology. The observed individual particles in the SEM were expected to be found as polycrystalline and hence their size was larger than the crystallite size obtained from X-ray peak broadening. SEM micrographs showed also a fine-grained microstructure with a uniform grain size distribution and a high percentage of porosity (Figure 4a, 4b and 4e). It was observed that lanthanum permits grain growth for samples 23% and 24 % La (Figure 4c, 4d), this is probably due to the preferable distribution of La in the boundary region. La segregation at grain boundaries and therefore inhibition of grain growth is also possible. According to the obtained microstructure, it was expected that the microstructure formed in PLT ceramics could enable better dielectric properties of the material. As grain size of the PLT was observed to be maximum for the sample with 23% La dopant, which would indicate its conformity with the XRD results, and thus it was expected to achieve the dielectric properties among other La dopant concentrations.

### 3.3. TEM analysis

Figure 5 presents the typical TEM images of the PLT powders with different La contents calcined at 1000 °C. According to TEM images, the PLT powders were heterogeneous, which may be the cause of the agglomeration of particles during their preparation. The primary particle sizes of the powder were determined by TEM analysis.

### 3.4. Optical properties

The prepared nanoparticles' optical properties were studied by a UV-Visible Spectrophotometer (UV-300II, TECHCOMP). Figure 5 presents the UV-Vis transmission spectra of the electrochemically synthesized

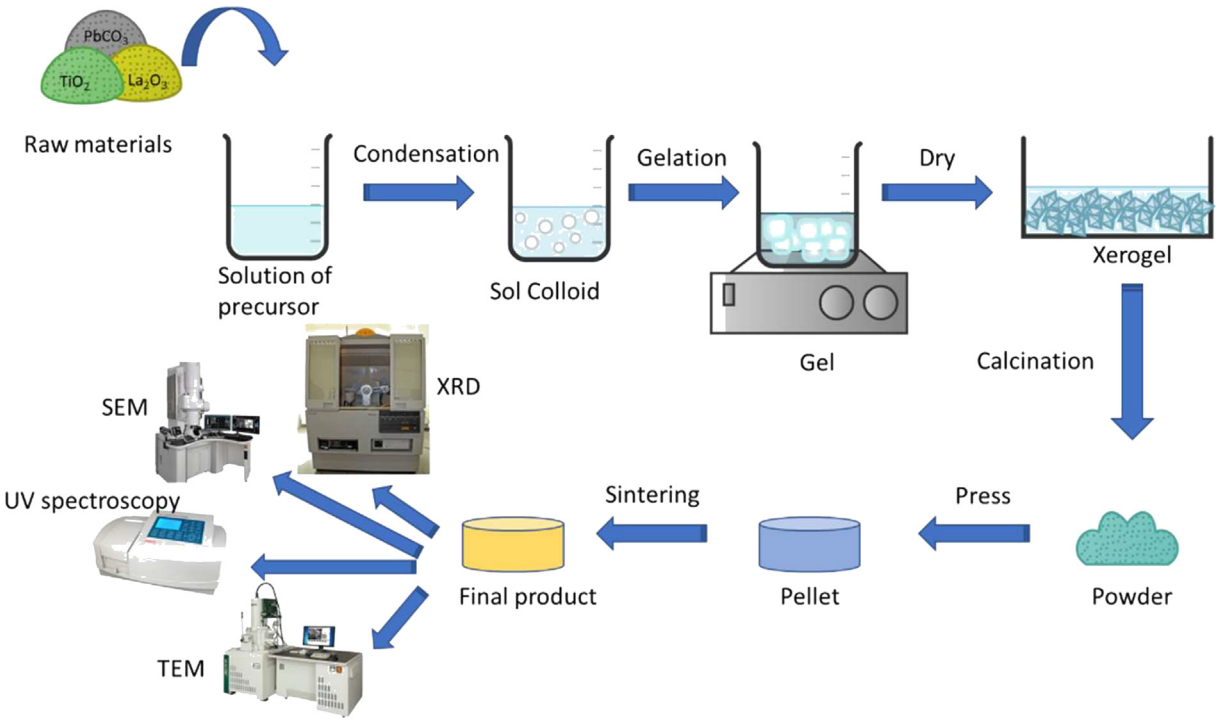


**Figure 1.** The block diagram of the sol-gel preparation method.

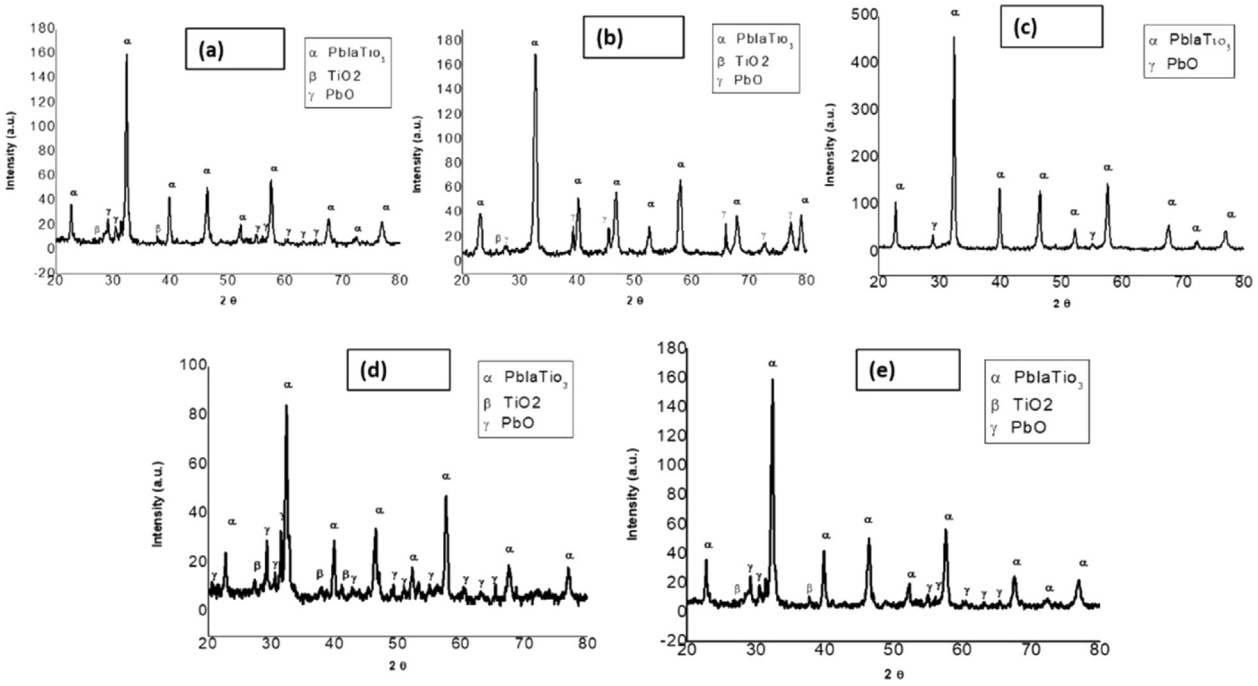


**Figure 2.** X-ray diffraction patterns of PLT ceramics annealed for 2 h at 1000 °C: x = (a) 0.21, (b) 0.22, (c) 0.23, (d) 0.24, and (e) 0.25.

nanoparticles in the 400–750 nm wavelength range at room temperature. The value of the optical gap $E_g^{opt}$ is calculated based on the Tauc plot [16]:

$$h\nu\alpha = (h\nu - E_g^{opt})^2 \quad (2)$$

where h is the Plank constant, $\nu$ is the frequency, and $E_g^{opt}$ α is the optical bandgap. The PLT bandgap Eg can be estimated by plotting $(\alpha h\nu)^2$ versus $h\nu$ and extrapolating the linear portion of the plot to $(\alpha h\nu)^2 = 0$ (as shown in Figure 6). The calculated bandgaps were 3.1, 3.26, 3.28, 3.08, and 3.12 for the PLT with 0.21, 0.22, 0.23,0.24 and 0.25% La, respectively.

Average particle sizes and the energy gap, calculated by the Scherrer's equation and the Tauc plot, respectively, are presented in Figure 7 as a function of the La concentration. The sample with 23% La possessed the largest grain size (49.6 nm) and the highest energy gap (4.5 eV) among all tested samples.

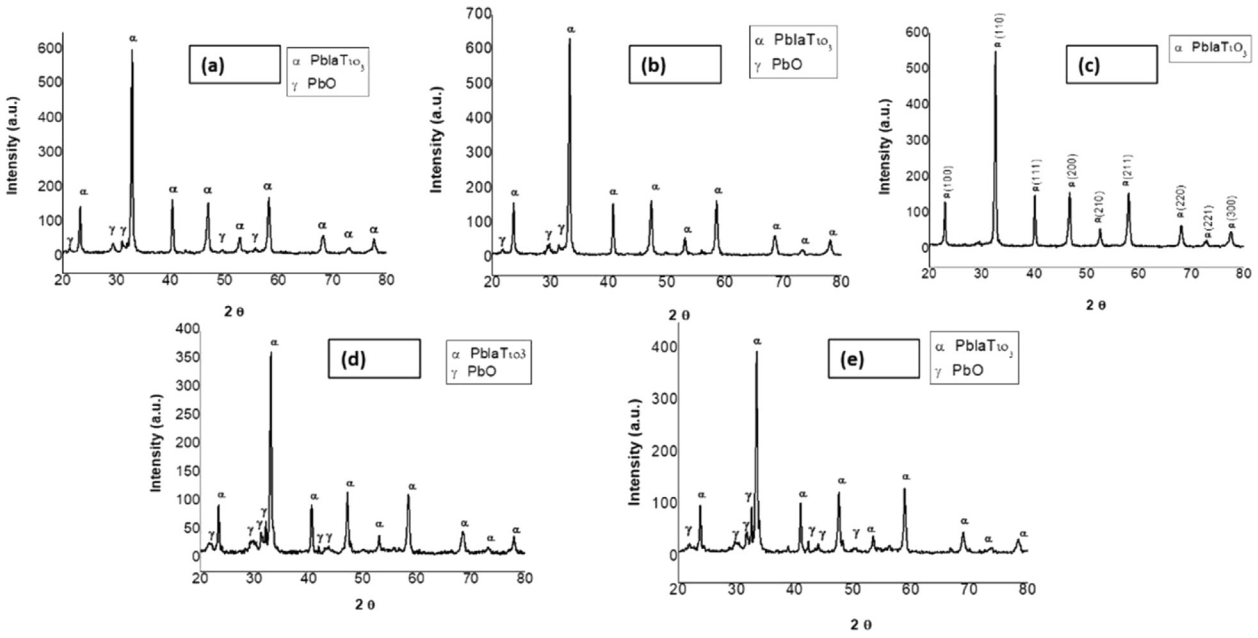


**Figure 3.** X-ray diffraction patterns of PLT ceramics annealed for 4 h at 1000 °C: x = (a) 0.21, (b) 0.22, (c) 0.23, (d) 0.24, and (e) 0.25.

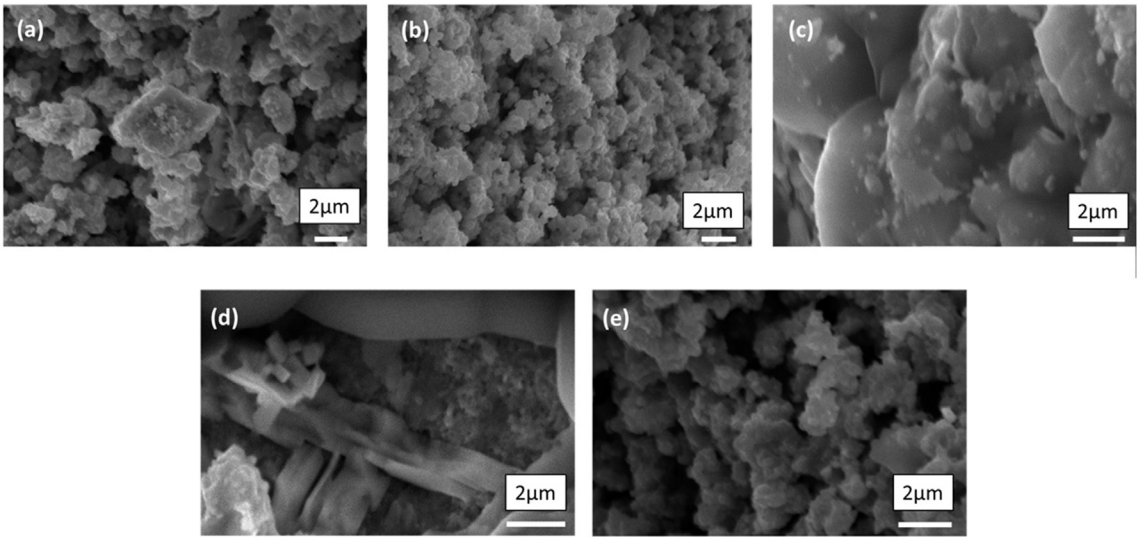


**Figure 4.** SEM images of $[(Pb_{1-x}\ La_x\ \square_{0.5x})]TiO_3$ ceramics sintered at 1000 °C: x = (a) 0.21, (b) 0.22, (c) 0.23, (d) 0.24, and (e) 0.25.

### 3.5. Dielectric properties of PLT nanoparticles

Dielectric studies of the PLT nanoparticles were conducted to analyze their reactions to an applied ac voltage (1 V) as a function of temperature and frequency. Figure 8 indicates the dielectric constant ($\varepsilon_r$) of the PLT ceramics as a function of temperatures at the frequency of 10 kHz. $\varepsilon_r$ increased gradually with the rise in temperature and reached the maximum value $\varepsilon_m$ at a particular temperature known as the Curie Temperature $T_m$. $\varepsilon_m$ values of PLT are listed in Table 1, showing that PLT with 23% La had the highest $\varepsilon_m$ (3649). The Curie Temperature $T_c$ and temperature corresponding to the maximum dielectric constant Tm for La-doped samples shifted towards low temperature.

It is recognized that all the ferroelectric materials dielectric permittivity over the Curie temperature follows the Curie–Weiss law:

$$1/\varepsilon_r = (T - T_c)/C \quad \text{where } T > T_c \tag{3}$$

where $T_c$ is Curie–Weiss temperature and C is the Curie–Weiss constant. It is observed that in part of the paraelectric phase at a temperature higher than $T_m$, $T_{cw}$ is the Burns Temperature. A deviation from Curie–Weiss law starting at $T_{cw}$ can be seen. The parameter that describes the deviation degree is defined as

$$\Delta T_m = T_{cw} - T_m \tag{4}$$

The Curie constant C was obtained as the slope of the curve of the inverse values of $\varepsilon_r$ vs. temperature (Figure 9). With an increasing La-dopant amount, the value of C increased. The highest C value ($5.2 \times 10^5$ K) was measured for the 23% La sample (Table 1). The C value is related to the grain size and porosity of the samples [35]. The

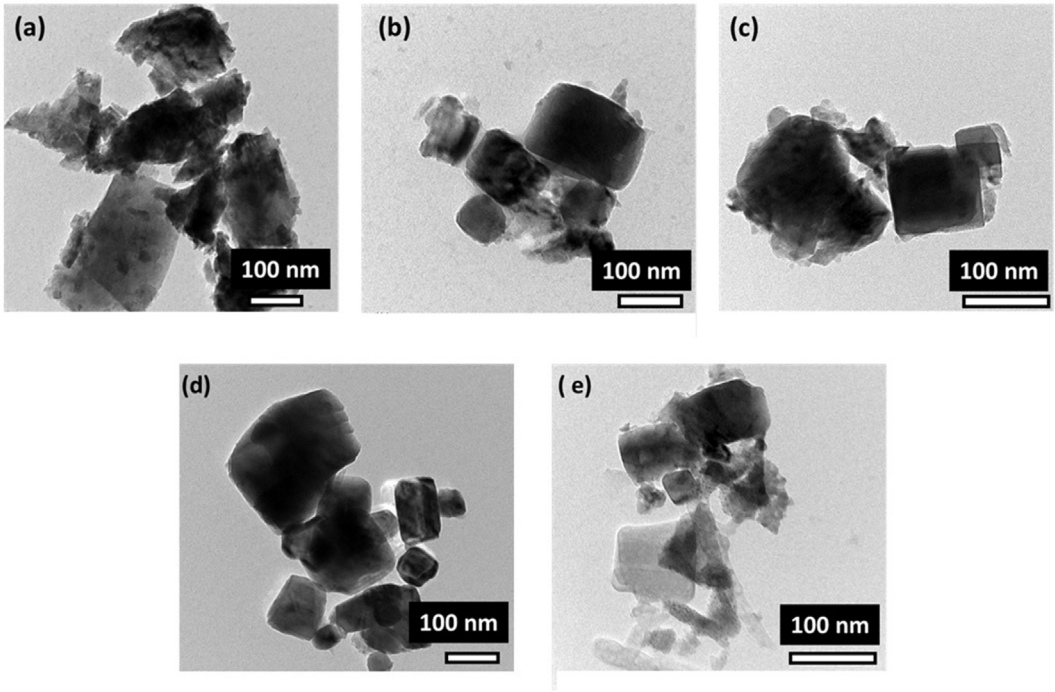


**Figure 5.** TEM images of $[(Pb_{1-x}\ La_x\ \square_{0.5x})]TiO_3$ ceramics sintered at 1000 °C: x = (a) 0.21, (b) 0.22, (c) 0.23, (d) 0.24, and (e) 0.25.

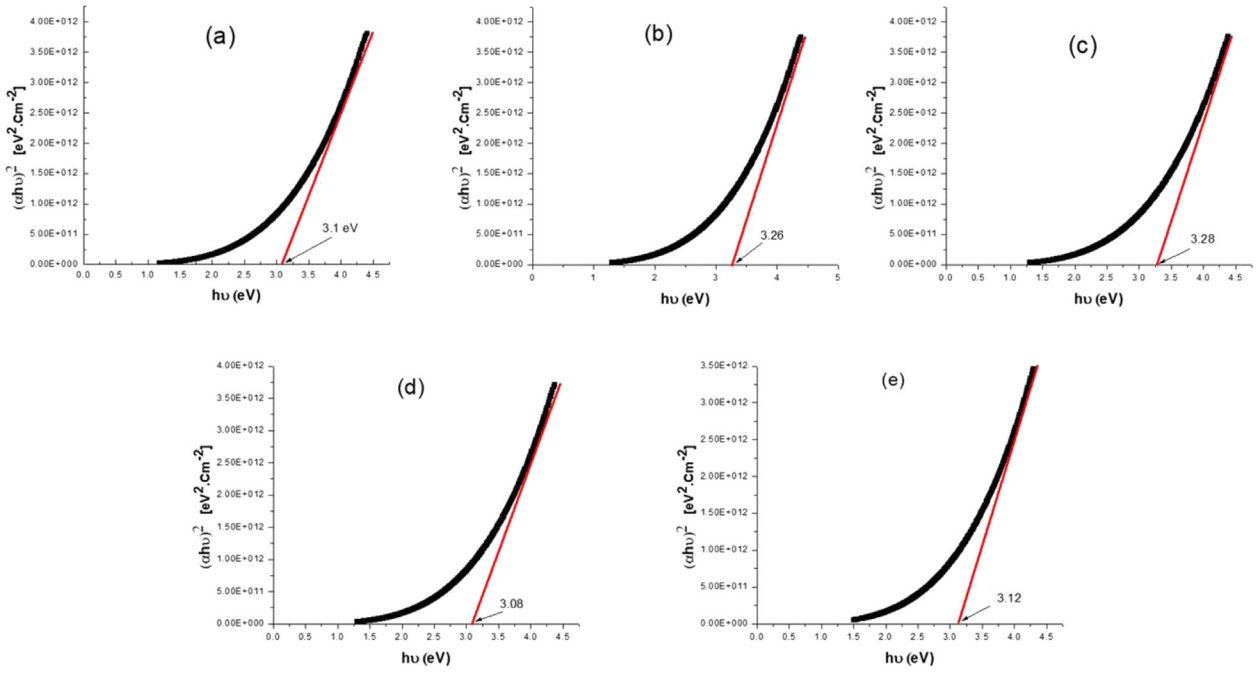


**Figure 6.** Energy gaps of PLT powders annealed at 1000 °C for 4 h x = (a) 0.21, (b) 0.22, (c) 0.23, (d) 0.24, and (e) 0.25.

transition temperature $T_c$ decreases linearly with the increasing La content.

The dielectric characteristics of the relaxor ferroelectric, different from the Curie–Weiss behavior, can be defined by an important modified equation of Curie–Weiss:

$$1/\varepsilon - 1/\varepsilon_m = (T - T_m)\,\gamma / C_1, 1 \le \gamma \le 2, \quad (5)$$

where $\gamma$ and $C_1$ are constants. The parameter $\gamma$ is used to obtain data on the character of the phase transition: when $\gamma = 1$ a normal Curie–Weiss law is obtained and $\gamma = 2$ describes a complete diffuse phase transition [36].

Plots of $\ln(1/\epsilon - 1/\epsilon_m)$ as a function of $\ln(T - T_m)$ for the tested PLT samples with deferent La concentrations are presented in Figure 10. Linear relationships were observed for all five samples. By fitting the data to Eq. (1), the critical exponent $\gamma$ representing the degree of diffuse transition was obtained as the slope of the fitting curve. At 10 kHz, $\gamma$ = 1.74, 2.61, 1.37, 1.83, and 1.04 for PLT ceramics with La concentration of 21%, 22%, 23%, 24%, and 25 %, respectively.

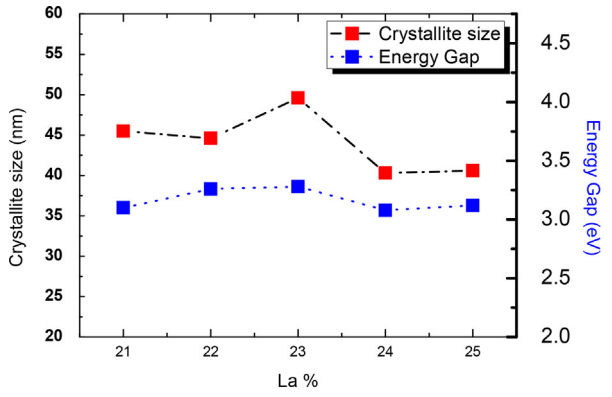


**Figure 7.** Crystallite sizes and energy gap of PLT powders with different La concentrations after annealing.

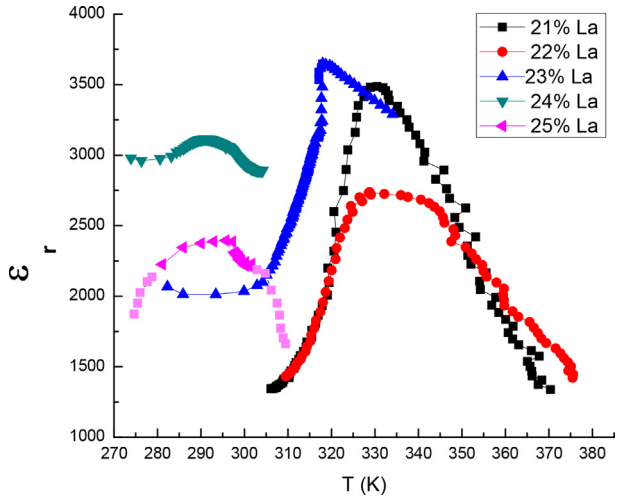


**Figure 8.** The temperature in Kelvin Vs the dielectric constant of $(Pb_{1-x}\ La_x\ \square_{0.5x})TiO_3$ single phase calcined at 1000 °C, where x = 0.21, 0.22, 0.23, 0.24, and 0.25.

Table 1 shows that $T_m$, $T_c$ and $T_{cw}$ decreases with increasing La-doping concentration, while ÄT$_m$ which illustrates the deviation degree from the Curie–Weiss law is fluctuated, it achieved its minimum value for 23% la and 25 %.

Understanding the tolerance factor assists in achieving the main developments of new compounds within the perovskite family. In order to classify the formation of perovskite-type compounds, Goldschmid expressed in the following tolerance factor t [37] was used:

$$t = \frac{r_{A+}r_O}{\sqrt{2}(r_B + r_O)} \quad (6)$$

Where $r_A$, $r_B$,$r_O$ are the effective ionic radii of A sites and B and the oxygen ion sites respectively. The average ionic radii of A-site are calculated using the following relation [38]:

$$r_A = \left[(1 - 1.5x)Pb^{2+}\right] + \left[x\left(La^{3+}\right)\right] + [0.5x(V)] \quad (7)$$

Where, $r_{Pb^{2+}} = 1.49$ Å, $r_{La^{3+}} = 1.36$ Å indicates Shannon's radii values. The mismatch between the A-site and B-site cations' bonding requirements in the $ABO_3$ perovskite is measured quantitatively by the Tolerance factor which reflects the distortion structure that contains the octahedral rotation and tilt. As the substituent radii $La^{3+}$ ion at A-site is lesser than Pb, the tilt and the centrosymmetric distortion reduce. As indicated in Table 2, the tolerance factor calculated values of the PLT samples decrease from 0.991 (as in x = 0.21) to 0.986 (as in x = 0.25). Hence, the general the structures tend to be in the perovskite structure as the calculated tolerance factor t ~ 1.

Figure 11 a show The PLT atomic distribution of unit cell. As illustrated in figure the $Ti^{4+}$ ions at the origin as $TiO_6$ octahedral. This octahedral distortion is assumed as a result of the covalent O-Ti-O bond displacement in the structure. Replacement of trivalent ions ($La^{3+}$) in the sites generally occupied by divalent ions ($Pb^{2+}$) has led to negative charge restitution in the PLT lattice and creation A-site– deficient structures. The distortion presence in the PLT crystallizing in the cubic perovskite structure was linked to structural defects as a result of the different doping mechanism [39].

Figure 11 b shows a centrosymmetric illustration of PLT ceramics. The VESTA software is used to model the Atomic structure PLT unit

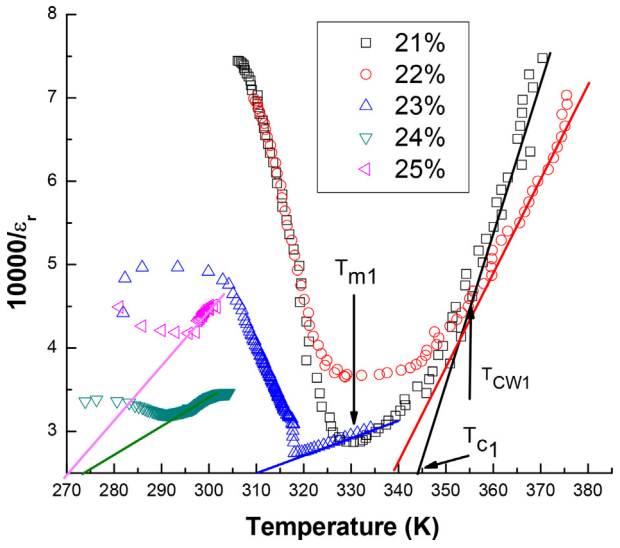


**Figure 9.** The relationship between the inverse dielectric permittivity (10000/$\varepsilon_r$) versus the temperature at 10 kHz. (The solid colored lines indicate the fitting curves based on the Curie–Weiss law for $(Pb_{1-x}\ La_x\ \square_{0.5x})\ TiO_3$ single-phase calcined at 1000 °C, where x = 0.21, 0.22, 0.23, 0.24, and 0.25.). Where $T_{c1}$,$T_{m1}$, $T_{cw1}$ is Curie–Weiss temperature, the temperature of permittivity maximum, and the Burns Temperature for -as for example- 21% La respectively.

**Table 1.** Values of the maximum dielectric permittivity ($\varepsilon_m$), the temperature corresponding to the maximum dielectric constant ($T_m$), Curie–Weiss temperature ($T_c$), the temperature above which the dielectric constant ($\varepsilon$) follows the Curie–Weiss law ($T_{cw}$), ($\Delta T_m = T_{cw} - \Delta T_m$) and the critical parameter ($\gamma$), Curie–Weiss constant (C) , Energy Gap and Crystallite size for PLT ceramic at different La% concentrations.

| Sample | $\varepsilon_m$ | $T_m$ (K) | $T_c$ (K) | $T_{cw}$ (K) | $\Delta T_m$ (K) | γ | C.$10^5$ K | Energy Gap (eV) | Crystallite size (nm) |
|---|---|---|---|---|---|---|---|---|---|
| 21% La | 3486 | 330 | 345 | 355 | 25 | 1.74 | 0.66 | 3.1 | 45.5 |
| 22% La | 2737 | 329 | 340 | 355 | 26 | 2.60 | 0.99 | 3.26 | 44.6 |
| 23% La | 3649 | 318 | 310 | 320 | 2 | 1.37 | 5.2 | 3.28 | 49.6 |
| 24% La | 3115 | 291 | 275 | 295 | 4 | 1.83 | 3.3 | 3.08 | 40.3 |
| 25% La | 2394 | 296 | 270 | 298 | 2 | 1.04 | 1.4 | 3.12 | 40.6 |

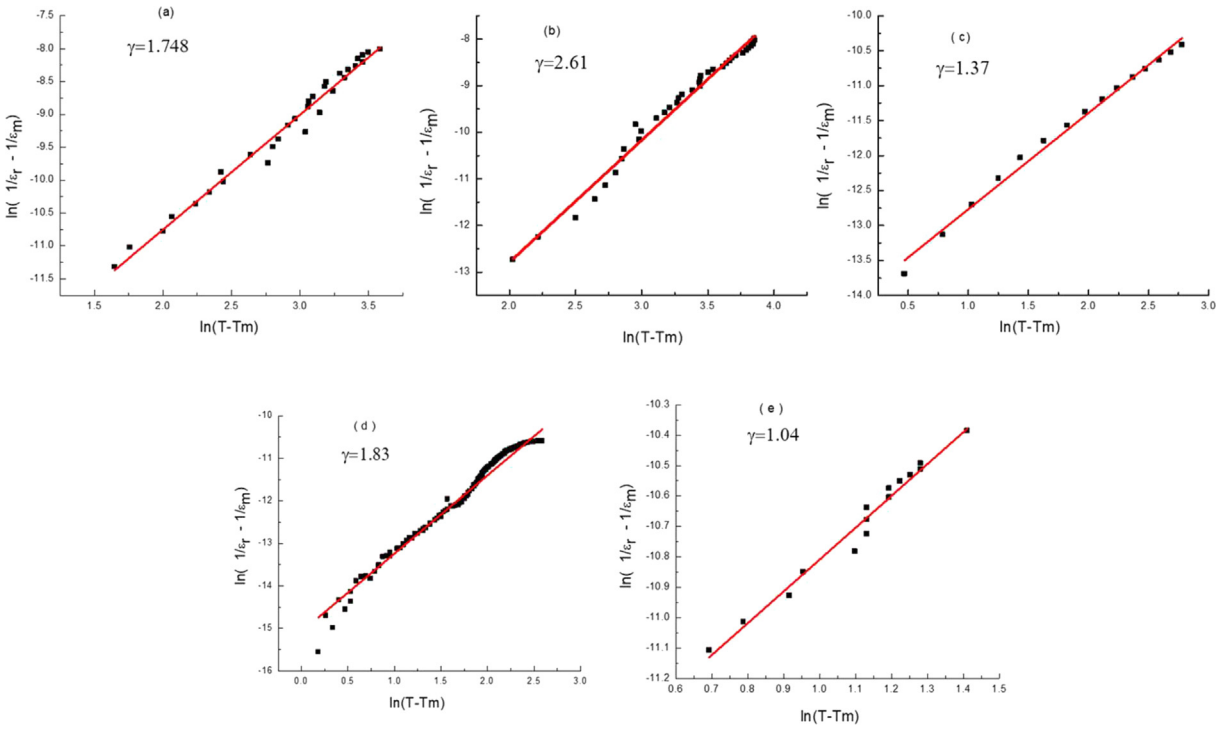


**Figure 10.** Ln $(1/\epsilon - 1/\epsilon_m)$ as a function of ln $(T - T_m)$ for different grain sizes: x = (a) 0.21, (b) 0.22, (c) 0.23, (d) 0.24, and (e) 0.25. [Symbols: experimental data, solid line: fits to Eq. (5)].

**Table 2.** The Tolerance factor (t) of La-doped lead titanate ceramics.

| Substitution (x) | 0.21 | 0.22 | 0.23 | 0.24 | 0.25 |
|---|---|---|---|---|---|
| Tolerance factor (t) | 0.991 | 0.99 | 0.988 | 0.987 | 0.986 |

cell perovskites [39]. Figure 11 (b) shows how the octahedral are connected at their corners to form a 3D simple cubic system, enclosing a large space busy by Pb or La atom. The structure can also be described by the Ti -O chains run in parallel lines with all three Cartesian coordinates.

It can be expected that $La^{3+}$ ions if possible, occupy the $Pb^{2+}$ site in the lead titanate ceramics due near ionic radii. Thus, increasing $La^{3+}$ ions concentration maybe causes the increase the functions as a donor leading to some single vacancies of A site in the lattice, which eases the movement of domain wall so as to improve the dielectric properties significantly [40] to reach the maximum at lanthanum concentration equal to 23%, then for more $La^{3+}$ concentrations (24% and 25 %) it can be expected that it leads to some double vacancies of A site in the lattice which will complicate movement of domain wall so as to minimize the dielectric properties.

As $La^{3+}$ substitutes a Pb ion in the lead titanate lattice and doping generally induced the creation of defects such as vacancies $V_{pb}$ and probably $V_{Ti}$ and $V_O$ in low concentrations. It was predictable that $La^{3+}$ as a smaller ion would stabilize the cubic structure as predicted by Goldschmidt's tolerance factor (calculated in Table 2.). The existence of La on a Pb site creates the tetragonal structure weaker and possible generation of Ti vacancies ($V_{Ti}$) destroys Ti-O-Ti linkages. This occurrence leads to a lowering of $T_C$ [41].

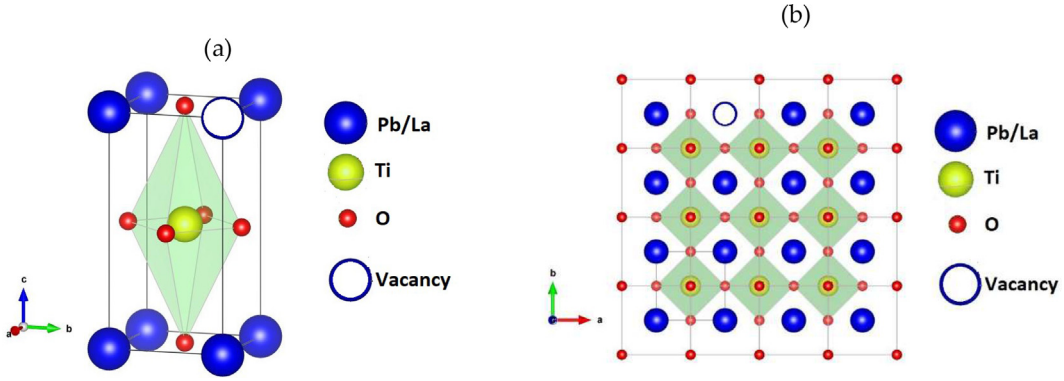


**Figure 11.** Atomic structure PLT unit cell perovskites. On the left, the positions of the ions in a tetragonal structure. On the right, the Pb/La atoms corner-sharing $TiO_6$ octahedra and oxygen vacancy migration path.

## 4. Conclusion

PLT nanoparticles with different La concentrations (i.e., 21%, 22%, 23%, 24%, and 25%) have been successfully prepared by the sol-gel method with different annealing times (i.e., 2 and 4 h) at the same sintering temperature of 1000 °C. In general, no secondary phases have been observed for the PLT with 23% La (PLT23) in its XRD spectrum. Structural, optical, and dielectric properties of the synthesized PLT have been studied. Sample PLT23 is distinguished from other PLT samples due to its relatively higher grain size (~49.6 nm), energy gap (~3.28 eV), Curie–Weiss constant (~5.2 × 105 K), and the maximum dielectric constant (~3649). The calculated values for the parameters (ΔTm, γ, Tc) approve its relaxor behavior. The Curie Temperature Tc and temperature corresponding to the maximum dielectric constant Tm decreases with increasing the La concentration. Goldschmidt's tolerance factor is calculated for the PLT samples, it decreases from 0.991 as in x = 21 to 0.986 for x = 0.25.

## Declarations

### *Author contribution statement*

M. Mostafa: Conceived and designed the experiments; Performed the experiments; Analyzed and interpreted the data; Contributed reagents, materials, analysis tools or data; Wrote the paper.

Z. A. Alrowaili: Contributed reagents, materials, analysis tools or data.

G. M. Rashwan: Performed the experiments; Analyzed and interpreted the data; Contributed reagents, materials, analysis tools or data.

M. K. Gerges: Analyzed and interpreted the data; Contributed reagents, materials, analysis tools or data.

### *Funding statement*

This research did not receive any specific grant from funding agencies in the public, commercial, or not-for-profit sectors.

### *Competing interest statement*

The authors declare no conflict of interest.

### *Additional information*

No additional information is available for this paper.

## Acknowledgements

The authors are thankful to technician members of Central laboratory, South Valley University, H. Mohamed,A. Ibrahem, N. Maghrabi,H. Barakat and F. Elrashedi for providing XRD and electron microscopic facilities.

## References

[1] L.B. Kong, T.S. Zhang, J. Ma, F. Boey, Progress in synthesis of ferroelectric ceramic materials via high-energy mechanochemical technique, Prog. Mater. Sci. 53 (2) (2007) 207–322.

[2] Luis K. Ono, Emilio J. Juarez-Perez, Yabing Qi, Progress on perovskite materials and solar cells with mixed cations and halide anions, ACS Appl. Mater. Interfaces 9 (2017) 30197–30246.

[3] Yichuan Chen, Linrui Zhang, Yongzhe Zhang, Hongli Gaoa, Hui Yan, Largearea perovskite solar cells – a review of recent progress and issues, RSC Adv. 8 (2018) 10489–10508.

[4] Jessada Khajonrit, Unchista Wongpratat, Pinit Kidkhunthod, Supree Pinitsoontorn, Santi Maensiri, Effects of Co doping on magnetic and electrochemical properties of BiFeO3 nanoparticles, J. Magn. Mag. Mater. 449 (2018) 423–434.

[5] K.W. Tan, D.T. Moore, M. Saliba, H. Sai, L.A. Estroff, T. Hanrath, H.J. Snaith, U. Wiesner, Thermally induced structural evolution and performance of mesoporous block copolymer-directed alumina perovskite solar cells, ACS Nano 8 (5) (2014) 4730–4739.

[6] J. Mendiola, B. Jiménez, C. Alemany, L. Pardo, L. Del Olmo, Influence of calcium on the ferroelectricity of modified lead titanate ceramics, Ferroelectrics 94 (1) (1989) 183–188.

[7] B. Jaffe, R. Cook, H. Jaffe, Piezoele. Ceramics, Academic Press, New York, 1971, p. 115.

[8] I. Szafraniak, M. Połomska, B.X.R.D. Hilczer, TEM and Raman scattering studies of $PbTiO_3$ nanopowders, Cryst. Res. Technol. 41 (6) (2006) 576–579.

[9] R. Wongmaneerung, A. Rujiwatra, R. Yimnirun, S. Ananta, Fabrication and dielectric properties of lead titanate nanocomposites, J. Alloys Compd. 475 (1-2) (2009) 473–478.

[10] I. Szafraniak-Wiza, B. Hilczer, E. Talik, A. Pietraszko, B. Malic, Ferroelectric perovskite nanopowders obtained by mechanochemical synthesis, Process. Appl. Ceram. 4 (3) (2010) 99–106.

[11] C. Chankaew, A. Rujiwatra, Hydrothermal synthesis of lead titanate fine powders at water boiling temperature, Chiang Mai J. Sci. 37 (1) (2010) 92–98.

[12] M. Lanki, A. Nourmohammadi, M.H. Feiz, A precise investigation of lead partitioning in sol-gel derived $PbTiO_3$ nanopowders, Ferroelectrics 448 (1) (2013) 123–133.

[13] K. Ishikawa, N. Okada, K. Takada, T. Nomura, M. Hagino, Crystallization and growth process of lead titanate fine particles from alkoxide-prepared powders, Jpn. J. Appl. Phys. 33 (6R) (2013) 3495.

[14] M.K. Gerges, M. Mostafa, G.M. Rashwan, Structural, optical and electrical properties of $PbTiO_3$ nanoparticles prepared by Sol-Gel method, Int. J. Res. Eng. Technol. 2 (4) (2013) 42–49.

[15] G.H. Haertling, Improved hot-pressed electrooptical ceramics in the (Pb, La)(Zr, Ti)$O_3$ system, J. Am. Ceram. Soc. 54 (6) (1971) 303–309.

[16] R. Takayama, Y. Tomita, K. Lijima, I. Ueda, Pyroelectric linear array infrared sensors made of c-axis-oriented La-modified PbTiO3 thin films, J. Appl. Phys. 63 (12) (1988) 5868–5872.

[17] G.A. Gamal, M.K. Gerges, M.A. Massaud, Influence of structure on Curie weiss constant of $[(Pb_{1-x}\ Sr_x)_{1-1.5z}La_z]TiO_3$ ceramics, Egypt. J. Solids 30 (1) (2007) 103–119.

[18] Z. Kutnjak, J. Petzelt, R. Blinc, The giant electromechanical response in ferroelectric relaxors as a critical phenomenon, Nature 441 (7096) (2006) 956–959.

[19] S. Zhang, W. Jiang, J.R. Meyer Jr., F. Li, J. Luo, W. Cao, Measurements of face shear properties in relaxor-$PbTiO_3$ single crystals, J. Appl. Phys. 110 (6) (2011) 64106.

[20] Y. Zhang, G. Gao, H.L.W. Chan, J. Dai, Y. Wang, J. Hao, Piezo-photonic effect-induced dual-mode light and ultrasound emissions from ZnS: Mn/PMN-PT thin-film structures, Adv. Mater. 24 (13) (2012) 1729–1735.

[21] W. Windsch, M.K. Gerges, D. Michel, H. Schlemmbach, A. Salzer, P. Reich, Spectroscopic and dielectric studies on lanthanum modified $PbTiO_3$ ceramics, Ferroelectrics 109 (1) (2012) 119–124.

[22] G.A. Gamal, M.K. Gerges, M.A. Massaud, Influence of structure on Curie weiss constant of $[(Pb_{1-x}\ Sr_x)_{1-1.5z}La_z]TiO_3$ ceramics, Egypt. J. Solids 30 (1) (2007) 103–119. http://egmrs.powweb.com/EJS/PDF/vol301/9-(862).pdf.

[23] L. Wu, C.C. Wei, T.S. Wu, C.C. Teng, Dielectric properties of modified PZT ceramics, J. Phys. C Solid State Phys. 16 (14) (1983) 2803.

[24] G. King, E.K. Goo, Effect of the c/a ratio on the domain structure in $(Pb_{1-x},Ca_x)TiO_3$, J. Am. Ceram. Soc. 73 (6) (1990) 1534–1539.

[25] C.C. Chan, Y.T. Hsieh, C.F. Yang, P.S. Cheng, Sintering and dielectric properties of Sr(Bi2Ta2)1-xTi4xO9 ceramics, Ceram. Int. 29 (5) (2003) 495–498.

[26] S.L. Swartz, T.R. Shrout, W.A. Schulze, L.E. Cross, Dielectric properties of lead-magnesium niobite ceramics, J. Am. Ceram. Soc. 67 (5) (1984) 311–314.

[27] M. Chen, X. Yao, L. Zhang, Grain size dependence of dielectric and field-induced strain properties of chemical prepared (Pb, La)(Zn, Sn, Ti)$O_3$ antiferroelectric ceramics, Ceram. Int. 28 (2) (2002) 201–207.

[28] B.S. Kang, S.K. Choi, Diffuse dielectric anomaly of $BaTiO_3$ in the temperature range of 400-700 °C, Solid State Commun. 121 (8) (2002) 441–446.

[29] S. Garcia, J. Portelles, F. Martinez, R. Fount, J.R. Quinones, Grain growth in polycrystalline $Ba_{0.5}Sr_{0.5}TiO_3$ ceramics prepared at different sintering times, Rev. Mex. Fis. 49 (1) (2003) 15–19.

[30] L. Szymczak, Z. Ujma, J. Handere, J. Kapusta, Sintering effects on dielectric properties of (Ba,Sr)TiO3 ceramics, Ceram. Int. 30 (6) (2004) 1003–1008.

[31] M.P. McNeal, S.J. Jang, R.E. Newnham, The effect of grain and particle size on the microwave properties of barium titanate ($BaTiO_3$), J. Appl. Phys. 83 (6) (2004) 3288–3297.

[32] M. Massaud, Khaled, A.S. Hussien, R. Reham, Effect of laser beam on structural, optical, and electrical properties of $BaTiO_3$ nanoparticles during sol-gel preparation, J. Korean Ceram. Soc. 55 (6) (2018) 581–589.

[33] X.G. Tang, Effect of grain size on the electrical properties of (Ba,Ca)(Zr,Ti)$O_3$ relaxor ferroelectric ceramics, J. Appl. Phys. 97 (3) (2005) 34109.

[34] T. Zhang, X. Huang, X. Tang, et al., Enhanced electrocaloric analysis and energy-storage performance of lanthanum modified lead titanate ceramics for potential solid-state refrigeration applications, Sci. Rep. 8 (2018) 396.

[35] Denghui Ji, ShunZhen Feng, Li Wang, Shuling Wang, Na Mula, Hong Zhang, CongMin Zhang, Xiuling Li, Regulatory tolerance and octahedral factors by using vacancy in APbI3 perovskites, Vacuum 164 (2019) 186–193.

[36] N. Abdelmoula, H. Chaabane, H. Khemakhem, R. Vonder Mühll, A. Simon, Relaxor or classical ferroelectric behavior in A-site substituted perovskite type $Ba_{1-x}(Sm_{0.5}Na_{0.5})_xTiO_3$, Solid State Sci. 8 (2006) 880–887.

[37] Y. Guaaybess, L. Zerhouni, E. El Moussafir, A. Laaraj, R. Adhiri, M. Moussetad, Effect of Ce and La substitution on dielectric properties of lead titanate ceramics, J. Mater. Environ. Sci. 6 (12) (2015) 3491–3495.
[38] V. Paunović, Lj. Živković, V. Mitić, Influence of rare-earth additives (La, Sm and Dy) on the microstructure and dielectric properties of doped $BaTiO_3$ ceramics, Sci. Sinter. 42 (2010) 69–79.
[39] K. Momma, F. Izumi, VESTA 3 for three-dimensional visualization of crystal, volumetric and morphology data, J. Appl.Crystallography 44 (2011) 1272. https://www.readcube.com/articles/10.1107/s0021889811038970.
[40] T. Zhang, X. Huang, X. Tang, et al., Enhanced electrocaloric analysis and energy-storage performance of lanthanum modified lead titanate ceramics for potential solid-state refrigeration applications, Sci. Rep. 8 (2018) 396.
[41] M.M. Vijatović Petrović, J.D. Bobića, R. Grigalaitis, B.D. Stojanović, J. Banysb, La-doped and La/Mn-co-doped barium titanate ceramics, Acta Phys. Pol., A 124 (2013).